

Mesonic decay constants in lattice NRQCD

B.D. Jones and R.M. Woloshyn

TRIUMF, 4004 Wesbrook Mall, Vancouver, British Columbia, Canada, V6T 2A3

(December 8, 1998)

Abstract

Lattice NRQCD with leading finite lattice spacing errors removed is used to calculate decay constants of mesons made up of heavy quarks. Quenched simulations are done with a tadpole improved gauge action containing plaquette and six-link rectangular terms. The tadpole factor is estimated using the Landau link. For each of the three values of the coupling constant considered, quarkonia are calculated for five masses spanning the range from charmonium through bottomonium, and one set of quark masses is tuned to the B_c . “Perturbative” and nonperturbative meson masses are compared. One-loop perturbative matching of lattice NRQCD with continuum QCD for the heavy-heavy vector and axial vector currents is performed. The data are consistent with $af_V \propto \sqrt{M_V a}$ and $f_{B_c} = 420(13)$ MeV.

PACS number(s): 12.38.Gc, 12.39.Jh, 13.20.Gd, 13.20.Jf

I. INTRODUCTION

The gross features of quarkonia are well described by quenched lattice NRQCD [1–3]. However, spin splittings between vector and pseudoscalar mesons tend to be underestimated—especially when relativistic corrections are included [4–6]. Using the quark model, spin splittings are due to a short-ranged Fermi-Breit interaction and essentially measure the square of the meson’s wave function at the origin. Since they are not well understood within lattice NRQCD it is of interest to investigate physical quantities which probe the same physics. This is provided by the mesonic decay constants which, in the quark model, are proportional to the wave function at the origin.

In this paper, the focus is on the vector decay constants of quarkonia and the pseudoscalar decay constant of the B_c meson. The calculated quarkonia constants can of course be compared with experiment—for bottomonium this provides a test of the wave function at the origin, which is not possible from the spin splitting since the η_b has not been observed yet. On the other hand, the B_c has only recently been discovered [7] and its decay constant is not measured; however, comparison between our results and previous lattice NRQCD and other model predictions can be made.

A previous study [8] of the vector decay constant found large corrections from the perturbative matching between the continuum and lattice currents. Another study [9] reported a rather imprecise value for simulations which included the order v^2 relativistic corrections of the vector current. Previous studies [10,11] of the B_c decay constant reported results which did not include matching or relativistic corrections in the current itself. In this paper we remove the leading finite lattice spacing errors in the fermion and gauge actions in a symmetric fashion and perform (1) more precise simulations with the inclusion of the order v^2 relativistically corrected currents and (2) one-loop matching between the lattice and continuum currents at lowest order in v^2 .

The paper is arranged as follows. In Sec. II lattice NRQCD is introduced and tadpole improvement is discussed. Continuum and lattice matrix elements are matched up via perturbation theory in this paper. Thus, in Sec. III lattice perturbation theory is set up. Appendix A lists the free gluon propagator and the integrand of the amputated axial vector correction. A discussion of the matching with continuum QCD is presented in Sec. IV (Appendix B shows the origin of the ‘ $1/v$ ’ terms in the continuum QCD result). A general discussion of lattice decay constants, along with our conventions, is presented in Sec. V, and finally our results are discussed in Sec. VI.

II. LATTICE NRQCD

The fermion NRQCD Lagrangian is discretized in a symmetric fashion with the leading finite lattice spacing errors in the spatial and temporal derivatives removed. All links are tadpole improved by dividing by u_0 , the average link in the Landau gauge. The choice of ‘Landau link’ over ‘average plaquette’ tadpole is made based on spin splitting studies of quarkonia [5] where improved scaling behavior was observed. Tadpole improvement in general improves the matching between perturbation theory and lattice simulations [12] (see Table I for our evidence for this). The fermion Lagrangian we use is

$$a\mathcal{L}_F = \psi_t^\dagger \psi_t - \psi_t^\dagger \left(1 - \frac{a\delta H}{2}\right)_t \left(1 - \frac{aH_0}{2n}\right)_t \frac{U_{4,t-1}^\dagger}{u_0} \left(1 - \frac{aH_0}{2n}\right)_{t-1} \left(1 - \frac{a\delta H}{2}\right)_{t-1} \psi_{t-1}, \quad (1a)$$

$$H_0 = -\frac{\Delta^{(2)}}{2m}, \quad \delta H = \frac{a^2 \Delta^{(4)}}{24m} - \frac{a \left(\Delta^{(2)}\right)^2}{16nm^2}, \quad (1b)$$

$$u_0 = \left\langle \frac{1}{3} \text{ReTr} U_\mu \right\rangle, \quad \partial_\mu A_\mu = 0. \quad (1c)$$

n is the stability parameter chosen to satisfy $n > 3/(ma)$. $\Delta^{(2)}$ is the gauge-covariant lattice Laplacian, and $\Delta^{(4)}$ is the gauge-covariant lattice quartic operator $(\sum_i D_i^4)$.¹

The above form of the fermion Lagrangian is convenient for defining Feynman rules. In lattice simulations the action leads to an evolution equation for the quark propagator of the form

$$G(\mathbf{x}, t) - \left(1 - \frac{a\delta H}{2}\right)_t \left(1 - \frac{aH_0}{2n}\right)_t \frac{U_{4,t-1}^\dagger}{u_0} \left(1 - \frac{aH_0}{2n}\right)_{t-1} \left(1 - \frac{a\delta H}{2}\right)_{t-1} G(\mathbf{x}, t-1) = a\delta^4(x), \quad (2)$$

where in this equation the source has been placed at the origin for convenience and $G(\mathbf{x}, t) = 0$ for $t < 0$.

The gauge action is tadpole improved with leading finite lattice spacing errors removed by six-link rectangles [13]:

$$S_G = \beta \sum_{\text{pl}} \frac{1}{3} \text{Re Tr} (1 - U_{\text{pl}}) - \frac{\beta}{20u_0^2} \sum_{\text{rt}} \frac{1}{3} \text{Re Tr} (1 - U_{\text{rt}}). \quad (3)$$

In lattice NRQCD meson masses can not be calculated directly from meson time correlation functions. However, using meson correlators at zero and nonzero momentum, a ‘kinetic’ mass is obtained by

$$E(\mathbf{p}) - E(\mathbf{0}) = \frac{\mathbf{p}^2}{2M_{kin}}, \quad (4)$$

where $E(\mathbf{p})$ is the simulation energy and the momentum \mathbf{p} is expressed in units of $2\pi/(Na)$, where ‘ Na ’ is the spatial extent of the lattice.

¹For the standard definitions of these lattice derivatives see for example Ref. [4].

III. PERTURBATIVE LATTICE NRQCD

The Feynman rules are derived from the actions of Eqs. (1) and (3) by making the replacement

$$U_\mu(x) \rightarrow \exp[ia_g A_\mu^a(x) T^a], \quad (5)$$

and expanding in g . This is not quite true because a gauge fixing term must be added to the gauge action before expanding in g . The standard covariant gauge-fixing term in lattice perturbation theory is

$$S_{GF} = \frac{1}{2\xi} \sum_x \left[\sum_\mu \{A_\mu^a(x) - A_\mu^a(x - \mu)\} \right]^2, \quad (6)$$

where the gluon field is to be expanded about the midpoint of the link:

$$A_\mu^a(x) = \int_{-\pi}^{\pi} \frac{d^4 q}{(2\pi)^4} A_\mu^a(q) \exp[iq \cdot (x + \mu/2)]. \quad (7)$$

To be complete, the fermion field in momentum space is defined by

$$\psi(x) = \int_{-\pi}^{\pi} \frac{d^4 p}{(2\pi)^4} \psi(p) \exp(ip \cdot x). \quad (8)$$

The gluon propagator follows from the quadratic part of $S_G + S_{GF}$. See Appendix A for its explicit form. Note that we use the Feynman gauge ($\xi = 1$) for perturbative lattice NRQCD self-energy and vertex corrections in this paper.

The coupling g in this perturbative identification [Eq. (5)] that we use is the so called “boosted coupling.” It is defined by rewriting the gauge action as

$$S_G = \frac{6}{g^2} \left[\frac{5}{3} \sum_{\text{pl}} \frac{1}{3} \text{Re Tr} \left(1 - \frac{U_{\text{pl}}}{u_0^4} \right) - \frac{1}{12} \sum_{\text{rt}} \frac{1}{3} \text{Re Tr} \left(1 - \frac{U_{\text{rt}}}{u_0^6} \right) \right]. \quad (9)$$

The $5/3$ and $-1/12$ are necessary to match the continuum action with its usual normalization. Comparing Eqs. (3) and (9) gives

$$\alpha = \frac{g^2}{4\pi} = \frac{5}{3} \left(\frac{6}{\beta u_0^4 4\pi} \right). \quad (10)$$

The benefits of using this boosted coupling can be seen by comparing the Landau link calculated nonperturbatively and perturbatively [12]: Define $u_0^{(2)}$ by

$$u_0 = 1 - \alpha u_0^{(2)}, \quad (11)$$

where u_0 is calculated nonperturbatively and $\alpha(\beta, u_0)$ is given by Eq. (10). Then compare with a perturbatively calculated $u_0^{(2)}$. This comparison is shown in Table I; the close agreement justifies the use of a boosted coupling.

Given the Feynman rules, the perturbative matching factors for the decay constants follow. We discuss this matching in detail in the next section. A “perturbative” meson mass can also be defined. For example in the equal mass case

$$M_{pert} = 2(mZ_m - E_0) + E_{sim} , \quad (12)$$

where Z_m is the mass renormalization and E_0 is the energy shift of a quark, and E_{sim} is the simulation energy extracted from the meson correlator. For details on how Z_m and E_0 are defined see Ref. [14].

IV. MATCHING WITH CONTINUUM QCD

Lattice NRQCD is an effective field theory that is fundamentally different from continuum QCD—the ultraviolet divergences in the matrix elements of interest are not the same. After renormalization, these differences are finite (since the infrared divergences are the same), but nevertheless in order to obtain continuum QCD results, a matching step must be performed. In this section we will focus on the *axial* vector current matching since the vector current case follows in a similar manner. Details of the axial vector current matching will be given, and in the end, results for the vector current case will also be shown.

In general for the annihilation decay of the B_c meson, matching leads to

$$\langle 0 | \bar{b} \gamma_0 \gamma_5 c | c \bar{b} \rangle \Big|_{cont} = Z_{match} \langle 0 | \bar{b} \gamma_0 \gamma_5 c | c \bar{b} \rangle \Big|_{lat} + \mathcal{O}(v^2) , \quad (13)$$

where v is the relative velocity of the \bar{b} and c . In performing this matching in this paper we neglect the order v^2 terms and calculate Z_{match} in one-loop perturbation theory. For this system $\alpha \sim .25$ and $v^2 \sim .2$: the expansion parameters are somewhat less than unity.

Although the matching can be done in one step,² we will use two steps for pedagogical reasons. The two step matching procedure starts with the matching of lattice NRQCD (lNRQCD) with continuum NRQCD (cNRQCD). Then continuum NRQCD is matched with continuum QCD (cQCD). In the end a one-loop formula, relating the simulated lattice NRQCD matrix element with its continuum counterpart of full QCD, is obtained.

We will use the following notation: the amputated vertex correction will be written as ‘ $g^2 \delta V$ ’; including the wave function renormalization factors, the total matrix element will be written as ‘ $1 + g^2 (\delta V + \delta Z_b/2 + \delta Z_c/2)$ ’ times the tree level amplitude; and we will use different regulators as given below—but our renormalization scheme is always the on-mass-shell scheme.

A. Matching lattice NRQCD with continuum NRQCD

The current matrix element is ultraviolet finite in NRQCD. However infrared divergences do arise, and in this subsection a gluon mass is used as a regulator. The matrix elements are calculated in the limit

²We performed the matching in one step also (matching continuum QCD directly with lattice NRQCD) and obtained the same result as what follows from the discussion below.

$$1 \gg \lambda/m_{red} \gg v \longrightarrow 0, \quad (14)$$

where λ is the gluon mass, v is the relative velocity and m_{red} is the reduced mass of the system,

$$1/m_{red} = 1/m_b + 1/m_c. \quad (15)$$

In continuum NRQCD it is convenient to work in the Coulomb gauge. The transverse gluons coupling to the quarks is suppressed by powers of v , so only the Coulomb exchange term needs to be considered. The wave function renormalization factor is

$$g^2 \delta Z \Big|_{cNRQCD} = -iC_f g^2 \int \frac{d^4 k}{(2\pi)^4} \frac{1}{(\mathbf{k}^2 + \lambda^2)(k_0 + \frac{\mathbf{k}^2}{2m} - i\varepsilon)^2}, \quad (16)$$

where $C_f = 4/3$. Performing the k_0 integration, we see that the result is trivial, $\delta Z \Big|_{cNRQCD} = 0$. The amputated vertex correction is

$$g^2 \delta V \Big|_{cNRQCD} = iC_f g^2 \int \frac{d^4 k}{(2\pi)^4} \frac{1}{(\mathbf{k}^2 + \lambda^2)(k_0 - \frac{\mathbf{k}^2}{2m_b} + i\varepsilon)(k_0 + \frac{\mathbf{k}^2}{2m_c} - i\varepsilon)}. \quad (17)$$

Performing the k_0 integration, we are left with

$$g^2 \delta V \Big|_{cNRQCD} = 2m_{red} C_f g^2 \int \frac{d^3 k}{(2\pi)^3} \frac{1}{(\mathbf{k}^2 + \lambda^2)\mathbf{k}^2} = \frac{2m_{red} g^2}{3\pi\lambda}. \quad (18)$$

In summary, for continuum NRQCD with the scales proportioned as in Eq. (14) through one loop we have

$$\langle 0 | \chi_b \psi_c | c\bar{b} \rangle \Big|_{cNRQCD} = \eta_b^\dagger \xi_c \left[1 + \frac{2m_{red} g^2}{3\pi\lambda} \right], \quad (19)$$

where ψ_c and χ_b are non-relativistic c and \bar{b} fields respectively.

Lattice NRQCD is defined in Euclidean space. However, since the zeroth component of the axial vector current is identical in Euclidean and Minkowski space, one can match directly with the continuum NRQCD result.³ The detailed form of the integrands is not given here (see Appendix A). Instead, we will just write the form of the final result

$$\langle 0 | \chi_b \psi_c | c\bar{b} \rangle \Big|_{lNRQCD} = \eta_b^\dagger \xi_c \left[1 + g^2 \left(\frac{2m_{red}}{3\pi\lambda} + \delta\bar{V}_{lat} + \delta Z_{lat}^c/2 + \delta Z_{lat}^b/2 \right) \right], \quad (20)$$

where the bar on δV_{lat} signifies the separation of the linear infrared divergence. The integration routine VEGAS [15] is used to perform the integrations. *Only infrared finite integrands are integrated with VEGAS.* We subtract and add low three-momentum versions (leaving the energy variable alone) of the original integrand, where the subtraction is chosen to (1) make

³For the vector case there is just a trivial factor of i that must be kept track of: $\gamma_{Eucl} = -i\gamma_{Mink}$.

the original integrand infrared finite and (2) leave a simpler infrared divergent integrand that can be integrated analytically (or else repeat the subtraction procedure on this new term also). In an equation

$$\int_{-\pi}^{\pi} d^4k I(k) = \int_{-\pi}^{\pi} d^4k \left[I(k) - I_{sub}(k) \theta(c^2 - \mathbf{k}^2) \right] + \int_{-\pi}^{\pi} d^4k I_{sub}(k) \theta(c^2 - \mathbf{k}^2), \quad (21)$$

where the step function is chosen for convenience in the analytic integration step—‘ c ’ is an arbitrary parameter less than ‘ π ’ (for example ‘1’ or ‘2’). In this way, the linear infrared divergence is analytically separated as we have written it in Eq. (20).

To conclude, divide Eq. (19) by Eq. (20). Through one loop with the scales proportioned as in Eq. (14)

$$\langle 0 | \chi_b \psi_c | c \bar{b} \rangle \Big|_{cNRQCD} = \langle 0 | \chi_b \psi_c | c \bar{b} \rangle \Big|_{INRQCD} \left[1 - g^2 \left(\delta \bar{V}_{lat} + \delta Z_{lat}^c / 2 + \delta Z_{lat}^b / 2 \right) \right], \quad (22)$$

where the remaining matching factor is infrared finite; however, a logarithmic divergence cancels between the remaining terms.

B. Matching continuum NRQCD with continuum QCD

First, our conventions for this subsection: dimensional regularization regulates the infrared (IR) and ultraviolet (UV) divergences;⁴ we will work with finite but small relative velocity v ; γ_5 is chosen to anticommute with all other gamma matrices; and as already mentioned, our renormalization scheme is the on-mass-shell scheme.

The necessary matching calculation for this subsection has been performed already by Braaten and Fleming [16]. Details are omitted here and can be found in Ref. [16]. However, one intermediate step of the calculation is discussed in Appendix B, that is, the origin of the ‘ $1/v$ ’ terms in the results.

The one-loop renormalization of the axial vector current matrix element consists of amputated vertex and wave function renormalization corrections. In continuum NRQCD it is convenient to use the Coulomb gauge. Here the wave function renormalization correction vanishes [see Eq. (16)], and the amputated vertex correction is UV finite. However there is an IR divergence. The full result in continuum NRQCD is

$$\langle 0 | \chi_b \psi_c | c \bar{b} \rangle \Big|_{cNRQCD} = \eta_b^\dagger \xi_c \left[1 + \frac{g^2}{6\pi^2} \left\{ \frac{\pi^2}{v} - \frac{i\pi}{v} \left(\frac{1}{\epsilon_{IR}} - 2 \log \frac{2m_{red}v}{\mu} + \log 4\pi - \gamma \right) \right\} \right]. \quad (23a)$$

In continuum QCD it is convenient to use the Feynman gauge. The matrix element is UV divergent, but these divergences cancel between the amputated vertex and wave function

⁴ The usual $D = 4 - 2\epsilon$ identification is made.

renormalization factors. There is a real IR divergence that also cancels, but the final result has an imaginary IR divergence. The full result in continuum QCD is

$$\langle 0 | \bar{b} \gamma_0 \gamma_5 c | c \bar{b} \rangle \Big|_{cQCD} = \bar{v}_b \gamma_0 \gamma_5 u_c \left[1 + \frac{g^2}{6\pi^2} \left\{ \frac{\pi^2}{v} + \frac{3}{2} \frac{m_b - m_c}{m_b + m_c} \log \frac{m_b}{m_c} - 3 - \frac{i\pi}{v} \left(\frac{1}{\epsilon_{IR}} - 2 \log \frac{2m_{red}v}{\mu} + \log 4\pi - \gamma \right) \right\} \right]. \quad (23b)$$

For the respective one-loop integrals to converge $\epsilon_{IR} < 0$ and $\epsilon_{UV} > 0$. Also, the diagrams are evaluated slightly above threshold,

$$q^2 = (m_b + m_c)^2 + m_b m_c v^2 + \mathcal{O}(v^4), \quad (24)$$

thus the \bar{b} and c can simultaneously go on-mass-shell giving rise to the imaginary contributions. Dividing these continuum QCD and NRQCD results [Eq. (23)], through one loop and for small v , gives for the final result

$$\langle 0 | \bar{b} \gamma_0 \gamma_5 c | c \bar{b} \rangle \Big|_{cQCD} = \langle 0 | \chi_b \psi_c | c \bar{b} \rangle \Big|_{cNRQCD} \left[1 + \frac{g^2}{6\pi^2} \left(\frac{3}{2} \frac{m_b - m_c}{m_b + m_c} \log \frac{m_b}{m_c} - 3 \right) \right], \quad (25)$$

where ‘ $\bar{v}_b \gamma_0 \gamma_5 u_c = \eta_b^\dagger \xi_c + \mathcal{O}(v^2)$ ’ has been used.

C. Matching lattice NRQCD with continuum QCD

In both of the previous two subsections the ultraviolet and infrared divergences canceled in the final result, thus the two steps can be combined. Substituting Eq. (22) into Eq. (25) gives for our final result

$$\langle 0 | \bar{b} \gamma_0 \gamma_5 c | c \bar{b} \rangle \Big|_{cQCD} = \langle 0 | \chi_b \psi_c | c \bar{b} \rangle \Big|_{lNRQCD} \left[1 + \frac{g^2}{6\pi^2} \left(\frac{3}{2} \frac{m_b - m_c}{m_b + m_c} \log \frac{m_b}{m_c} - 3 \right) - g^2 \left(\delta \bar{V}_{lat} + \delta Z_{lat}^c / 2 + \delta Z_{lat}^b / 2 \right) \right], \quad (26)$$

which as already mentioned is the same result we obtained by directly matching lattice NRQCD with continuum QCD in one step with the scales proportioned as in Eq. (14).

As promised, the result for the vector case will also be given. The procedure is the same as for the axial vector, and the result is very similar—take the previous with equal quark masses and ‘ $-3 \rightarrow -4$ ’:

$$\langle 0 | \bar{Q} \gamma Q | Q \bar{Q} \rangle \Big|_{cQCD} = \langle 0 | \chi_Q \sigma \psi_Q | Q \bar{Q} \rangle \Big|_{lNRQCD} \left[1 + \frac{g^2}{6\pi^2} (-4) - g^2 \left(\delta \bar{V}_{lat} + \delta Z_{lat}^Q \right) \right]. \quad (27)$$

We will use the following notation to report these matching contributions:

$$\langle 0 | J | M \rangle \Big|_{cQCD} = Z_{\text{match}} \langle 0 | J | M \rangle \Big|_{lNRQCD}. \quad (28)$$

Tables II and III show our results.

V. DECAY CONSTANTS

A meson propagator is given by

$$\begin{aligned} G(\mathbf{p}, t) &= \left\langle \sum_{\mathbf{x}} \exp[-i\mathbf{p} \cdot (\mathbf{x} - \mathbf{x}_0)] J(\mathbf{x}, t) J^\dagger(\mathbf{x}_0, t_0) \right\rangle \\ &= \left\langle \sum_{\mathbf{x}} \exp[-i\mathbf{p} \cdot (\mathbf{x} - \mathbf{x}_0)] \text{Tr} \left[(\Gamma_x G_{xx_0}) (G_{xx_0} \Gamma_{x_0})^\dagger \right] \right\rangle, \end{aligned} \quad (29)$$

where the trace is over spin and color, and G_{xx_0} is the quark propagator of Eq. (2). $J(\mathbf{x}, t) = \chi_x \Gamma_x \psi_x$ is a non-relativistic current with $\Gamma_x = \Omega_x \omega_x$, where Ω_x interpolates the meson of interest⁵ and ω_x is a smearing operator chosen in a gauge-covariant fashion:

$$\omega_x = [1 + \epsilon \Delta^{(2)}(x)]^{n_s}. \quad (30)$$

We set $\epsilon = 1/12$ and tune the smearing parameter n_s to maximize the overlap with the state of interest. The range 7–30 for n_s was found to be sufficient, with the P-wave requiring about twice as much smearing as the S-wave and the smearing parameter increasing for decreasing quark mass.

The asymptotic form of this non-relativistic meson propagator is

$$G(\mathbf{p}, t) \xrightarrow{t-t_0 \rightarrow \infty} |\langle 0 | J(0) | \mathbf{p} \rangle|^2 \exp[-E(\mathbf{p})(t - t_0)]. \quad (31)$$

In continuum Minkowski notation, this current matrix element for a pseudoscalar and vector at rest is related to the respective decay constant by

$$\langle 0 | \bar{b} \gamma_0 \gamma_5 c | B_c \rangle = \frac{if_{B_c} M_{B_c}}{\sqrt{2M_{B_c}}}, \quad (32a)$$

$$\langle 0 | \bar{Q} \boldsymbol{\gamma} Q | V \rangle = \frac{if_V M_V \boldsymbol{\epsilon}}{\sqrt{2M_V}}, \quad (32b)$$

where $\boldsymbol{\epsilon}$ is a polarization vector and for matching purposes a non-relativistic norm is assumed.

Simulations are performed with order v^2 relativistic corrections included in the currents. The relativistically corrected interpolating operator for a non-relativistic vector meson is given by

$$\Omega_V^{rel} = \sigma_i + \frac{1}{8m^2} \left(\Delta^{(2)\dagger} \sigma_i + \sigma_i \Delta^{(2)} \right) - \frac{1}{4m^2} \left(\boldsymbol{\sigma} \cdot \boldsymbol{\Delta}^\dagger \right) \sigma_i \left(\boldsymbol{\sigma} \cdot \boldsymbol{\Delta} \right), \quad (33)$$

where $\boldsymbol{\Delta}$ is the gauge-covariant symmetric lattice derivative and $\Delta^{(2)}$ is the gauge-covariant lattice Laplacian. For the B_c the relativistically corrected interpolating operator is

$$\Omega_{B_c}^{rel} = 1 + \frac{\Delta^{(2)}}{8m_{red}^2}. \quad (34)$$

⁵ $\Omega_x = I$, $\boldsymbol{\sigma}$, and $\boldsymbol{\Delta}$ for the 1S_0 , 3S_1 , and 1P_1 states respectively.

Our final decay constants are reported using the following notations: Let ‘src’ represent L (local) or S (smeared). ‘X’ is 1P_1 , PS (pseudoscalar), or V (vector). Three correlators are of interest:

$$\begin{aligned}
(1) \quad C_X^L &\equiv \left\langle \sum_{\mathbf{x}} J_X^L(\mathbf{x}, t) J_X^{L\dagger}(\mathbf{x}_0, t_0) \right\rangle \equiv Z_X^L \exp[-E_X^L(t - t_0)] , \\
(2) \quad C_X^S &\equiv \left\langle \sum_{\mathbf{x}} J_X^L(\mathbf{x}, t) J_X^{S\dagger}(\mathbf{x}_0, t_0) \right\rangle \equiv Z_X^S \exp[-E_X^S(t - t_0)] , \\
\text{and } (3) \quad C_X^{S,rel} &\equiv \left\langle \sum_{\mathbf{x}} J_X^{L,rel}(\mathbf{x}, t) J_X^{S\dagger}(\mathbf{x}_0, t_0) \right\rangle \equiv Z_X^{S,rel} \exp[-E_X^{S,rel}(t - t_0)] , \quad (35)
\end{aligned}$$

where $J_X^{L,rel}(\mathbf{x}, t) = \chi_x \Omega_X^{rel} \psi_x$ and the right-hand-side of these equations assumes $t \gg t_0$. Given this, we report two forms of decay constants:

$$\frac{f_X M_X}{\sqrt{2M_X}} = a^{-\frac{3}{2}} Z_{\text{match}} \sqrt{Z_X^L} \quad (36)$$

$$\text{and } \frac{f_X^{rel} M_X}{\sqrt{2M_X}} = a^{-\frac{3}{2}} Z_{\text{match}} \frac{\sqrt{Z_X^L} Z_X^{S,rel}}{Z_X^S} , \quad (37)$$

where f_X^{rel} includes the order v^2 relativistic corrections in the currents and Z_{match} is the perturbative matching factor of Eq. (28). The spirit of these definitions is from Ref. [17].

VI. RESULTS AND DISCUSSION

Tables IV and V show the simulation parameters and compare M_{pert} and M_{kin} . The lattice spacing is fixed by the splitting between S- and P-wave states which is taken to be 458 MeV for all simulations. For each coupling, five quark masses spanning the range from charmonium through bottomonium are used, and one set of quark masses is tuned to the B_c which we take to be 6.35 GeV for the spin averaged ground state.

The data sample includes 1200 quenched gauge field configurations at $\beta = 7.4$ ($10^3 \times 16$), and 1600 configurations at $\beta = 7.2$ and 7.3 ($8^3 \times 14$). A standard Cabbibo-Marinari pseudo heat bath is used to generate the gauge-field configurations. After 4000 thermalizing sweeps, the number of updates between measurements is 30. Autocorrelation times for the correlation functions are checked and satisfy $\tau \lesssim \frac{1}{2}$. Multiple sources ($N/2$) along the spatial diagonal are used to measure the local-smeared meson correlators with the number of smearing steps optimized to have the best overlap with the state of interest. Single exponential fits to the correlation functions are used to get the best estimates of the masses and decay constants. Effective mass plots are generated and used to choose the interval in which to do the fits. In all cases acceptable Q values are obtained. All statistical errors are estimated by the bootstrap method with twice as many bootstrap ensembles as there are configurations. As expected, simulation energies from L-L, L-S, and Lrel-S correlators are all consistent with each other.

Fig. 1 shows our main result for quarkonia:

$$af_V \propto \sqrt{M_V a} . \quad (38)$$

For a tabular form of this information see Table VI. This square-root dependence is quite interesting. Shortly after the discovery of charm, Yennie [18] noticed this same dependence from empirical data:

$$\frac{\Gamma_{e\bar{e}}^V}{e_q^2} \sim \text{constant} \sim 12 \text{ keV} \quad (39)$$

for light through heavy ground-state vector mesons (e_q is the quark charge in units of e). This is the same as our data since the leptonic width is proportional to $e_q^2 \frac{f_V^2}{M_V}$. A final note on this result: a *linear (Coulomb)* potential implies a *constant (linear)* dependence on the meson mass for the decay constant, so our data is consistent with a superposition of the two potentials.

In order to compare with experimental values of quarkonia we use results from Fig. 1 with masses nearest the physical J/ψ and Υ masses. However, the masses are not tuned precisely to the experimental values (see Table V). For example, the $\beta = 7.2$ decay constants should be larger according to the derived $af_V \propto \sqrt{M_V a}$ dependence. With this caveat, Figs. 2 and 3 show the comparison of our calculated decay constants with empirical values. Previous work on spin splittings would lead us to expect decay constants smaller than experimental values and this is what we find although the 10–15% underestimation (with the order v^2 relativistically corrected currents) may be a bit less than what one might have anticipated. As expected—since $v_c^2 \sim .3$ and $v_b^2 \sim .1$ —the shift from the order v^2 relativistic corrections in the currents is approximately three times as big for charmonium as compared to bottomonium.

The main B_c (spin averaged ground state ~ 6.35 GeV; see Table IV) results are shown in Fig. 4. The same information is in Table VII. In Fig. 5 a comparison with previous lattice results [10,11] for f_{B_c} combined with a partial list of other model results [21–25] is shown. Our final result, 420(13) MeV, is taken from the $\beta = 7.4$ data point ($a \sim .16$ fm).

This is an initial study of decay constants made up of heavy quarks which systematically includes removal of the leading finite lattice spacing errors in the action, and measures the effects of the leading relativistic corrections in the vector and axial vector currents. The current matrix elements are matched with continuum QCD through one-loop in perturbation theory at lowest order in v^2 . After removal of the leading finite lattice spacing errors in the action we find these matching corrections to be small. This is shown in Tables II and III: 10% for the J/Ψ ; 5% for the Υ ; and less than 1% for the B_c .

ACKNOWLEDGMENTS

We thank R. Lewis, N. Shakespeare, and H. Trottier for useful discussions. We also thank H. Trottier for the use of his quark propagator code. This work is supported by the Natural Sciences and Engineering Research Council of Canada.

APPENDIX A: GLUON PROPAGATOR AND δV_{LAT} FOR THE B_C

The gluon propagator follows from the quadratic part of $S_G + S_{GF}$. In the Feynman gauge ($\xi = 1$) the gluon propagator is [19] (λ is our gluon mass)

$$D_{\mu\nu}(k) = D_{\nu\mu}(k) = \frac{1}{\hat{k}^2} \frac{1}{\hat{k}^2 + \lambda^2} \left[\hat{k}_\mu \hat{k}_\nu + \sum_\sigma (\hat{k}_\sigma \delta_{\mu\nu} - \hat{k}_\nu \delta_{\mu\sigma}) \hat{k}_\sigma A_{\sigma\nu}(k) \right], \quad (\text{A1})$$

with ($c_1 = -1/12$)

$$A_{\mu\nu}(k) = A_{\nu\mu}(k) = (1 - \delta_{\mu\nu}) \Delta(k)^{-1} \left[(\hat{k}^2)^2 - c_1 \hat{k}^2 \left(2 \sum_\rho \hat{k}_\rho^4 + \hat{k}^2 \sum_{\rho \neq \mu, \nu} \hat{k}_\rho^2 \right) + c_1^2 \left\{ \left(\sum_\rho \hat{k}_\rho^4 \right)^2 + \hat{k}^2 \sum_\rho \hat{k}_\rho^4 \sum_{\tau \neq \mu, \nu} \hat{k}_\tau^2 + (\hat{k}^2)^2 \prod_{\rho \neq \mu, \nu} \hat{k}_\rho^2 \right\} \right], \quad (\text{A2})$$

where

$$\Delta(k) = \left(\hat{k}^2 - c_1 \sum_\rho \hat{k}_\rho^4 \right) \left[\hat{k}^2 - c_1 \left\{ (\hat{k}^2)^2 + \sum_\tau \hat{k}_\tau^4 \right\} + \frac{1}{2} c_1^2 \left\{ (\hat{k}^2)^3 + 2 \sum_\tau \hat{k}_\tau^6 - \hat{k}^2 \sum_\tau \hat{k}_\tau^4 \right\} \right] - 4c_1^3 \sum_\rho \hat{k}_\rho^4 \prod_{\tau \neq \rho} \hat{k}_\tau^2. \quad (\text{A3})$$

The usual

$$\hat{k}_\mu = 2 \sin(k_\mu/2) \quad (\text{A4})$$

and

$$\hat{k}^2 = 4 \sum_{\mu=1}^4 \sin^2(k_\mu/2) \quad (\text{A5})$$

definitions have been made. Also note that although we are working in the Feynman gauge here, $D_{\mu\nu}$ is *not* diagonal in the Lorentz indices.

The self-energy renormalization is performed as described by Morningstar in [14]. The vertex corrections follow in a similar manner. We will not write down all the Feynman rules here, but rather will do a particular example: the one-loop amputated vertex correction of the axial vector current at lowest order in v^2 in lattice NRQCD for the “free B_c ” system. In the notation of Eq. (20), this is $g^2 \delta V_{lat}$. This is a standard vertex correction: the axial vector current creates a c and \bar{b} which then exchange a gluon between them. The one-loop amputated vertex correction of the axial vector current at lowest order in v^2 in lattice NRQCD for the “free B_c ” system is

$$g^2 \delta V_{lat} = \frac{4}{3} g^2 \int_{-\pi}^{\pi} \frac{d^4 k}{(2\pi)^4} \frac{D_{\mu\nu}(k) N_{\mu\nu}}{\Delta_c(-k) \Delta_b(k)}; \quad (\text{A6})$$

the inverse propagator of the c is (F_c and E_c are defined below; n_c is a stability parameter)

$$\Delta_c(-k) = 1 - \exp(ik_4)F_c^{2n_c}(k)E_c^2(k) ; \quad (\text{A7})$$

the inverse propagator of the \bar{b} is (F_b and E_b are defined below; n_b is a stability parameter)

$$\Delta_b(k) = 1 - \exp(-ik_4)F_b^{2n_b}(k)E_b^2(k) ; \quad (\text{A8})$$

$D_{\mu\nu}$ is the above gluon propagator; and $N_{\mu\nu}$, a product of one gluon emission and absorption vertices, will be written below. There are no external momenta in Eq. (A6) because at lowest order in v^2 the three-momenta of the c and \bar{b} are set to zero. Also recall that the mass has been subtracted from the energies as part of the definition of NRQCD. In the above inverse quark propagators

$$F(k) = 1 - \frac{\hat{\mathbf{k}}^2}{4mn} \quad (\text{A9})$$

and

$$E(k) = 1 - \sum_{i=1}^3 \frac{\hat{k}_i^4}{48m} + \frac{(\hat{\mathbf{k}}^2)^2}{32nm^2} , \quad (\text{A10})$$

for the particular c and \bar{b} masses and stability parameters. The definitions

$$\hat{k}_i = 2 \sin(k_i/2) \quad (\text{A11})$$

and

$$\hat{\mathbf{k}}^2 = 4 \sum_{i=1}^3 \sin^2(k_i/2) \quad (\text{A12})$$

have been made. The final piece is $N_{\mu\nu}$. It is defined as

$$D_{\mu\nu}N_{\mu\nu} = N_T + N_S + N_{ST} , \quad (\text{A13})$$

where the ‘S’ and ‘T’ subscripts signify ‘spatial’ and ‘temporal’ components respectively.⁶ These three terms are

$$\begin{aligned} (1) \quad N_T &= D_{44}(k)E_b(k)E_c(k)F_b^{n_b}(k)F_c^{n_c}(k) , \\ (2) \quad N_S &= \sum_{i,j=1}^3 D_{ij}(k)N_{ij} , \\ \text{and } (3) \quad N_{ST} &= \sum_{i=1}^3 D_{i4}(k)(N_{i4} + N_{4i}) , \end{aligned} \quad (\text{A14})$$

where

⁶ Recall that our gluon propagator is not diagonal in Lorentz indices—hence the spatial-temporal terms.

$$\begin{aligned}
N_{ij} = \sin(k_i/2) \sin(k_j/2) & \left[\frac{1}{2m_c n_c} E_c(k) S_{n_c}^c(0, k) \{1 + \exp(ik_4) F_c^{n_c}(k)\} \right. \\
& \left. + 2K_i^c(0, k) \{1 + \exp(ik_4) F_c^{2n_c}(k) E_c(k)\} \right] \\
& \times \left[\frac{1}{2m_b n_b} E_b(k) S_{n_b}^b(0, k) \{1 + \exp(-ik_4) F_b^{n_b}(k)\} \right. \\
& \left. + 2K_j^b(0, k) \{1 + \exp(-ik_4) F_b^{2n_b}(k) E_b(k)\} \right] , \tag{A15}
\end{aligned}$$

$$S_n(p, k) = \sum_{\alpha=1}^n F^{\alpha-1}(p) F^{n-\alpha}(k) , \tag{A16}$$

$$K_i(p, k) = \frac{1}{48m} (\hat{p}_i^2 + \hat{k}_i^2) - \frac{1}{32nm^2} (\hat{\mathbf{p}}^2 + \hat{\mathbf{k}}^2) , \tag{A17}$$

$$\begin{aligned}
N_{i4} = & \left[\frac{1}{2m_c n_c} \sin(k_i/2) E_c(k) S_{n_c}^c(0, k) \{1 + \exp(ik_4) F_c^{n_c}(k)\} \right. \\
& \left. + 2 \sin(k_i/2) K_i^c(0, k) \{1 + \exp(ik_4) F_c^{2n_c}(k) E_c(k)\} \right] \\
& \times \left[i \exp(-ik_4/2) E_b(k) F_b^{n_b}(k) \right] , \tag{A18}
\end{aligned}$$

and

$$N_{4i} = N_{i4}^* |_{b \leftrightarrow c} . \tag{A19}$$

The specification of the integrand of Eq. (A6) is now complete.

APPENDIX B: ONE-LOOP AXIAL VECTOR CORRECTION

This Appendix analyzes the origin of the ‘ $1/v$ ’ terms in Eq. (23). First the NRQCD correction in Eq. (23a) is discussed, and then we move on to the QCD correction in Eq. (23b).

The NRQCD correction in Eq. (23a): The integral of interest here is the complete one-loop amputated axial vector correction of continuum NRQCD. The integral is straightforward and so we will not go into details here. Its integration is clearly described around Eqs. (14)–(16) of BF.⁷ Note that the result is entirely ‘ $1/v$ ’ terms [compare with Eq. (18)].

Now we discuss the correction in Eq. (23b). The integral of interest is the *infrared divergent piece* of the one-loop amputated axial vector correction in continuum QCD (the other pieces are not discussed here because their integration is straightforward). The complete amputated vertex correction is written in Eq. (11) of BF.⁸ The term of interest is the first part of the first term in this equation:

$$\Lambda_{IR} = \frac{64\pi i\alpha_s}{3} \int_0^1 dx \int_0^{1-x} dy \mu^{2\epsilon} \int \frac{d^D k}{(2\pi)^D} \frac{2p \cdot p'}{[k^2 - (xp' - yp)^2 + i\epsilon]^3}. \quad (\text{B1})$$

The 4-momentum of the \bar{b} is $p = (\sqrt{\mathbf{p}^2 + m_b^2}, \mathbf{p})$, and in the center-of-mass frame the 4-momentum of the c is $p' = (\sqrt{\mathbf{p}^2 + m_c^2}, -\mathbf{p})$. After integrating over k , changing variables to $s = x + y$ and $t = x/s$, and then integrating over s (as described in BF), the result is

$$\Lambda_{IR} = -\frac{2\alpha_s}{3\pi} m_b m_c \int_0^1 dt \frac{1}{\Delta_t - i\epsilon} \left[\frac{1}{\epsilon_{IR}} + \log \left(\frac{\tilde{\mu}^2}{\Delta_t - i\epsilon} \right) \right] [1 + \mathcal{O}(v^2)] + \mathcal{O}(\epsilon_{IR}), \quad (\text{B2})$$

where the usual $D = 4 - 2\epsilon_{IR}$ replacement has been made; for the s -integral to converge, ϵ_{IR} has to be negative; $\tilde{\mu}^2 = 4\pi\mu^2/e^\gamma$; and Δ_t is given by

$$\Delta_t = q^2(t - t_+)(t - t_-), \quad (\text{B3})$$

where

$$q^2 = (p + p')^2 = (m_b + m_c)^2 + m_b m_c v^2 + \mathcal{O}(v^4) \quad (\text{B4})$$

$$\begin{aligned} \text{and } t_{\pm} &= \frac{1}{q^2} \left[m_b^2 + p \cdot p' \pm \sqrt{(p \cdot p')^2 - m_b^2 m_c^2} \right] \\ &= \frac{m_b \pm m_{red} v}{m_b + m_c} + \mathcal{O}(v^2). \end{aligned} \quad (\text{B5})$$

Recall $1/m_{red} = 1/m_b + 1/m_c$. The origin of the ‘ $1/v$ ’ terms is seen by rewriting

$$\frac{m_b m_c}{\Delta_t - i\epsilon} = \frac{m_b m_c}{q^2(t_+ - t_-)} \left(\frac{1}{t - t_+ - i\epsilon} - \frac{1}{t - t_- + i\epsilon} \right), \quad (\text{B6})$$

⁷In this Appendix we will take “Ref. [16]” \rightarrow “BF”.

⁸BF’s notation is used in this Appendix. To convert to our notation take $\Lambda \rightarrow g^2 \delta V$ and $\alpha_s \rightarrow g^2/(4\pi)$.

and noting that

$$\frac{m_b m_c}{q^2(t_+ - t_-)} = \frac{1}{2v} + \mathcal{O}(v); \quad (\text{B7})$$

Note that the $\mathcal{O}(v^2)$ terms of Eq. (B5) cancel in the difference:

$$t_+ - t_- = \frac{2m_{red}v}{m_b + m_c} + \mathcal{O}(v^3). \quad (\text{B8})$$

To proceed with the integration, we find Lewin's book on polylogarithms [20] helpful. More specifically, we use the following three equations:

$$\int_0^u \frac{\log(a+bt)}{c+et} dt = \frac{1}{e} \log\left(\frac{ae-bc}{e}\right) \log\left(\frac{c+eu}{c}\right) - \frac{1}{e} \text{Li}_2\left[\frac{b(c+eu)}{bc-ae}\right] + \frac{1}{e} \text{Li}_2\left(\frac{bc}{bc-ae}\right), \quad bc-ae \neq 0, \quad (\text{B9a})$$

$$\text{Li}_2(x \pm i\varepsilon) \stackrel{x \leq -1}{=} \frac{\pi^2}{3} - \frac{1}{2} \log^2(x) \pm i\pi \log(x) - \left[\frac{\left(\frac{1}{x}\right)}{1^2} + \frac{\left(\frac{1}{x}\right)^2}{2^2} + \frac{\left(\frac{1}{x}\right)^3}{3^2} + \dots \right], \quad (\text{B9b})$$

and

$$\text{Li}_2(x) \stackrel{x \leq -1}{=} -\frac{\pi^2}{6} - \frac{1}{2} \log^2(-x) - \left[-\frac{\left(\frac{1}{-x}\right)}{1^2} + \frac{\left(\frac{1}{-x}\right)^2}{2^2} - \frac{\left(\frac{1}{-x}\right)^3}{3^2} + \dots \right], \quad (\text{B9c})$$

where a, b, c , and e may be complex, but x is real. $\text{Li}_2(z)$ is the dilogarithm function nicely elucidated in Ref. [20].

The integration of Eq. (B2) is now straightforward with result (as $v \rightarrow 0$)

$$\Lambda_{IR} = \frac{2\alpha_s}{3\pi} \left[\frac{1}{\epsilon_{IR}} - 2 + 2 \log \frac{\tilde{\mu}}{m_b + m_c} - 2 \frac{m_{red}}{m_b} \log \frac{m_{red}}{m_c} - 2 \frac{m_{red}}{m_c} \log \frac{m_{red}}{m_b} + \frac{\pi^2}{v} - \frac{i\pi}{v} \left(\frac{1}{\epsilon_{IR}} - 2 \log \frac{2m_{red}v}{\tilde{\mu}} \right) \right], \quad (\text{B10})$$

where recall $\log(\tilde{\mu}^2) = \log(\mu^2) + \log(4\pi) - \gamma$. Note that all the '1/v' terms of the full answer [Eq. (23b)] are here, as was to be shown. The *imaginary* '1/ε_{IR}' term is also here, but there appears to be an extra *real* '1/ε_{IR}' term. The fact that this is not an "extra term" is seen after including the wave function renormalization [Eq. (10) of BF]:

$$\sqrt{Z_Q} = 1 + \frac{2\alpha_s}{3\pi} \left[-\frac{1}{4\epsilon_{UV}} - \frac{1}{2\epsilon_{IR}} + \frac{3}{2} \log \frac{m_Q}{\tilde{\mu}} - 1 \right]; \quad (\text{B11})$$

both the \bar{b} and c contribute one of these factors which results in the cancelation of the *real* '1/ε_{IR}' term of Eq. (B10). After including both of these wave function renormalization factors and the complete amputated vertex correction, the result is Eq. (23b) as mentioned in the body of the paper.

REFERENCES

- [1] G.P. Lepage *et al.*, Phys. Rev. D **46**, 4052 (1992).
- [2] C.T.H. Davies *et al.*, Phys. Rev. D **50**, 6963 (1994).
- [3] C.T.H. Davies *et al.*, Phys. Rev. D **52**, 6519 (1995).
- [4] H.D. Trottier, Phys. Rev. D **55**, 6844 (1997).
- [5] N.H. Shakespeare and H.D. Trottier, Phys. Rev. D **58**, 034502 (1998).
- [6] T.R. Klassen, Proceedings of 16th International Symposium on Lattice Field Theory, **hep-lat/9809174**, 1998.
- [7] CDF collaboration, F. Abe *et al.*, submitted to Phys. Rev. D, **hep-ex/9804014**, 1998.
- [8] C.T.H. Davies and B.A. Thacker, Phys. Rev. D **48**, 1329 (1993).
- [9] G.T. Bodwin *et al.*, Phys. Rev. Lett. **77**, 2376 (1996).
- [10] C.T.H. Davies *et al.*, Phys. Lett. B **382**, 131 (1996).
- [11] S. Kim, Report No. SNU-TP-95-088, **hep-lat/9511010**, 1995 (unpublished).
- [12] G.P. Lepage and P.B. Mackenzie, Phys. Rev. D **48**, 2250 (1993).
- [13] M. Lüscher and P. Weisz, Comm. Math. Phys. **97**, 59 (1985); *Erratum* **98**, 433 (1985).
- [14] C.J. Morningstar, Phys. Rev. D **48**, 2265 (1993).
- [15] G.P. Lepage, J. Comp. Phys. **27**, 192 (1978).
- [16] E. Braaten and S. Fleming, Phys. Rev. D **52**, 181 (1995).
- [17] K-I. Ishikawa *et al.*, Phys. Rev. D **56**, 7028 (1997).
- [18] D.R. Yennie, Phys. Rev. Lett. **34**, 239 (1975); J.J. Sakurai, Physica A **96**, 300 (1979).
- [19] P. Weisz and R. Wohlert, Nucl. Phys. B **236**, 397 (1984); *Erratum* **247**, 544 (1984).
- [20] L. Lewin, *Polylogarithms and Associated Functions* (North Holland, New York, 1981).
- [21] S.S. Gershtein *et al.*, Phys. Rev. D **51**, 3613 (1995).
- [22] S.S. Gershtein *et al.*, Proceedings of Workshop on Heavy Quark Physics IV, **hep-ph/9803433**, 1998.
- [23] L.P. Fulcher, **hep-ph/9806444**, 1998.
- [24] A. Abd El-Hady *et al.*, **hep-ph/9807225**, 1998.
- [25] E.J. Eichten and C. Quigg, Phys. Rev. D **49**, 5845 (1994).

FIGURES

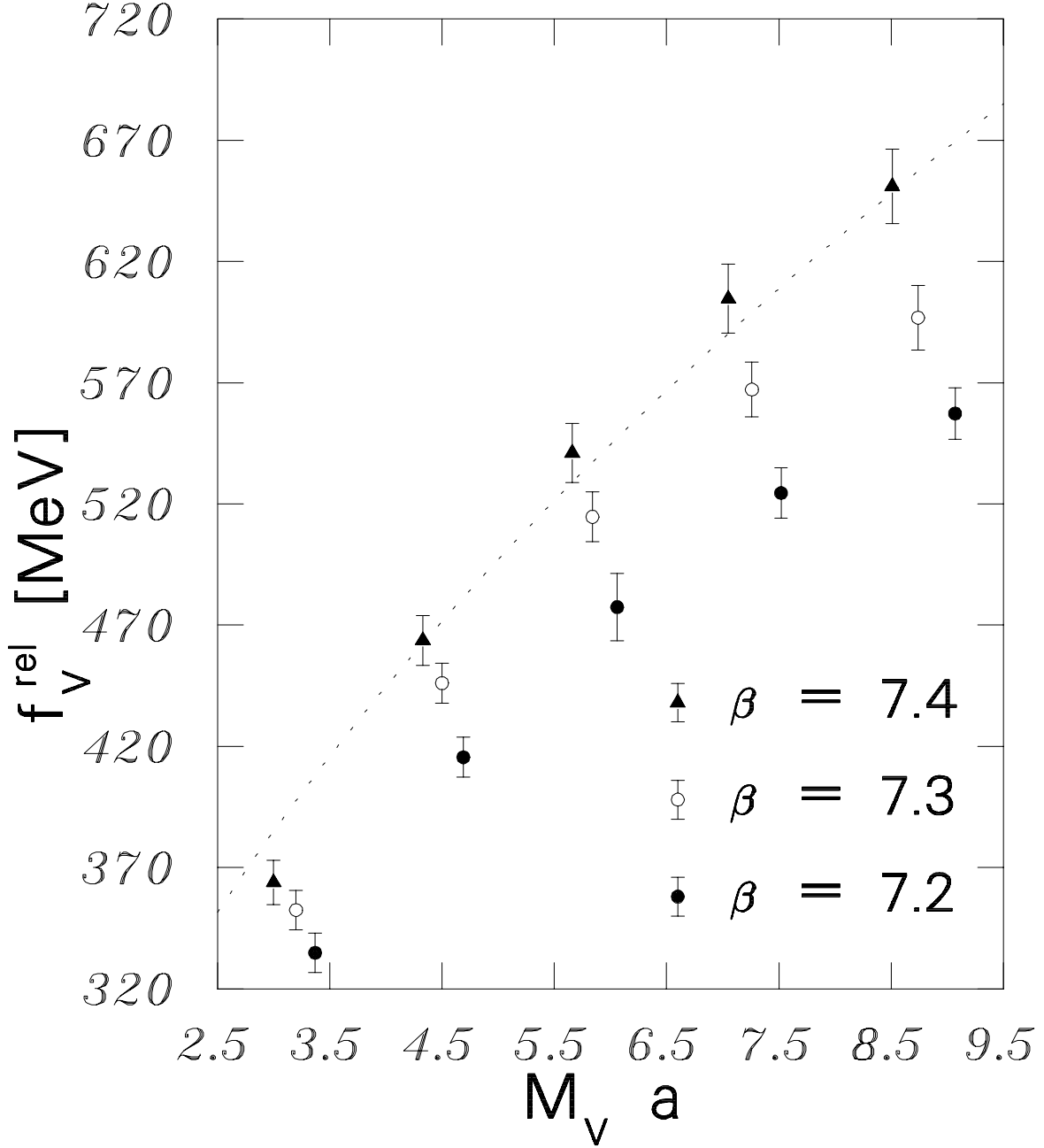


FIG. 1. Meson mass dependence of the order v^2 relativistically corrected vector decay constants of quarkonia including the one-loop perturbative matching. The dotted line is proportional to $\sqrt{M_V a}$.

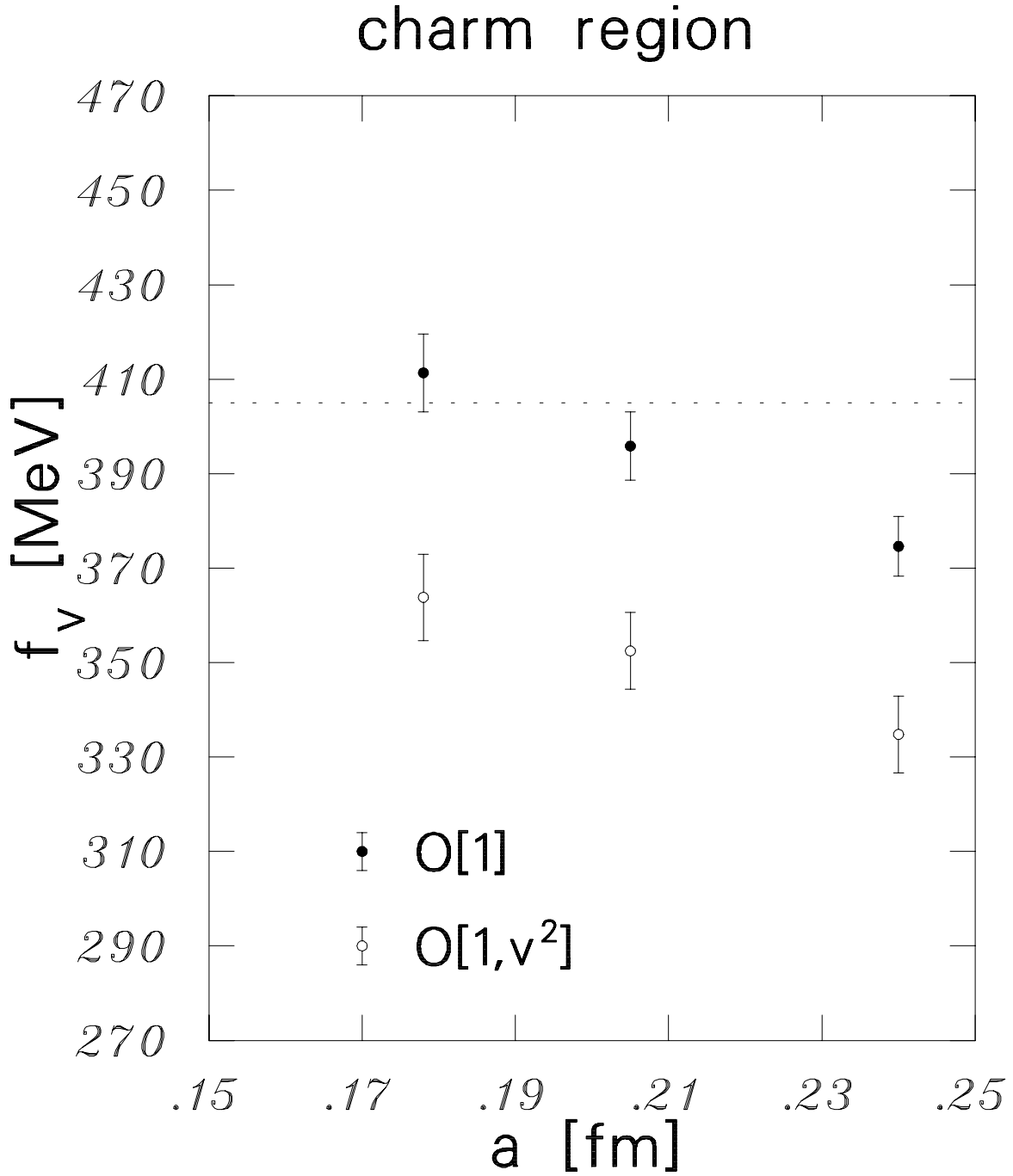


FIG. 2. The calculated vector decay constant of charmonium (including the perturbative matching) at different values of the lattice spacing with and without the relativistic corrections in the current. The dotted line is the experimental result.

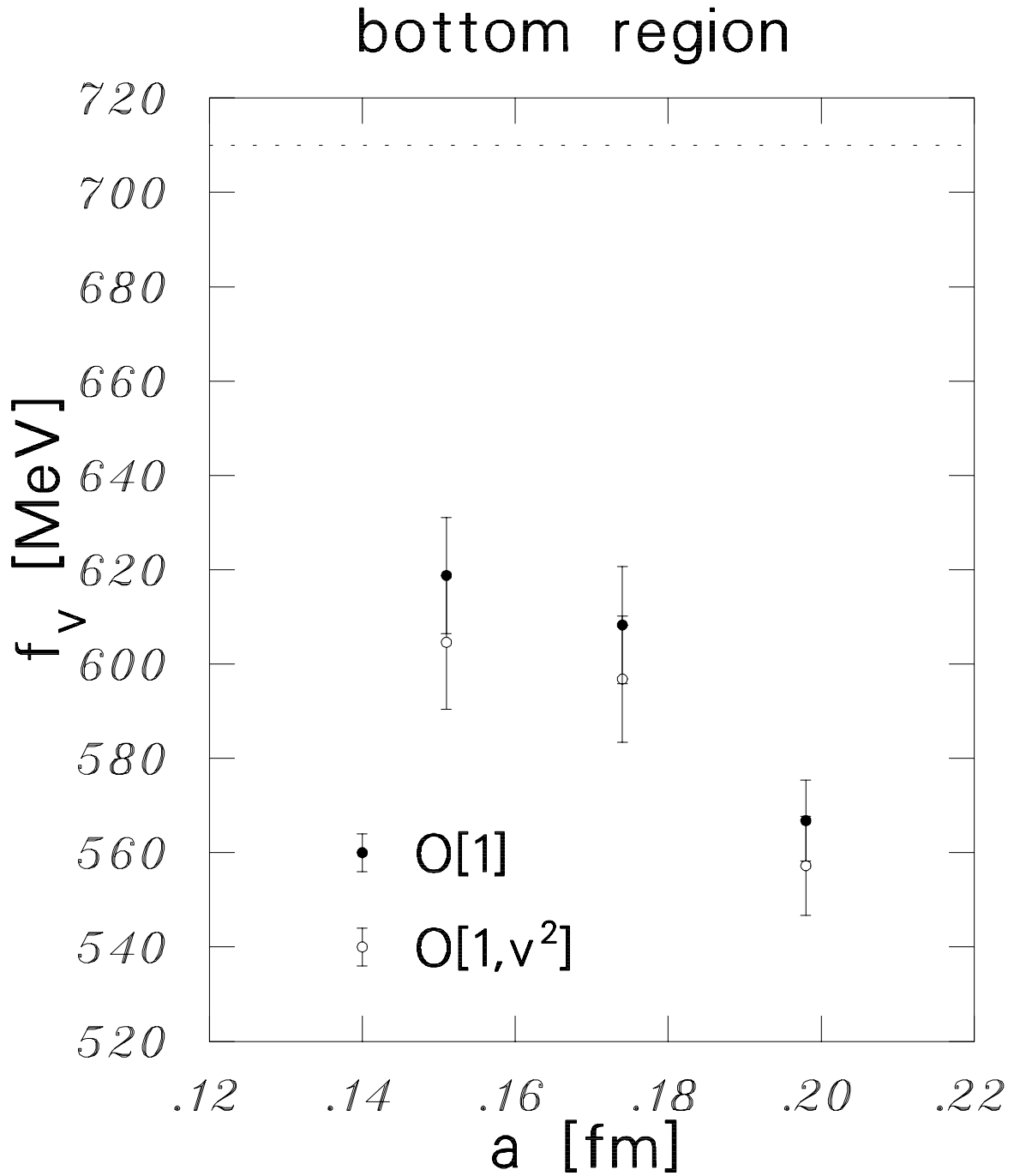


FIG. 3. The calculated vector decay constant of bottomonium (including the perturbative matching) at different values of the lattice spacing with and without the relativistic corrections in the current. The dotted line is the experimental result.

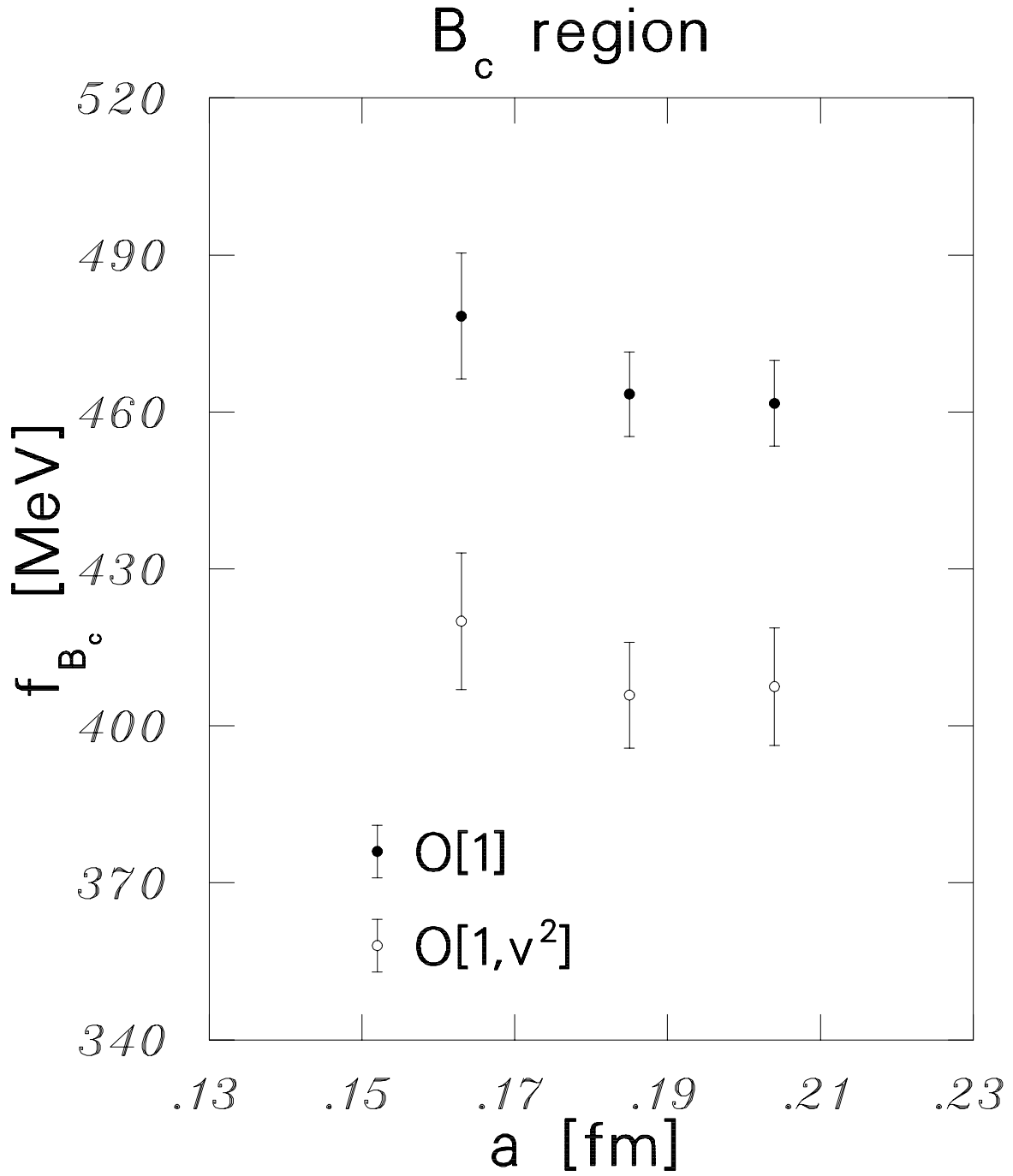


FIG. 4. Scaling behavior of the B_c decay constant (including the perturbative matching) with and without the relativistic corrections in the current.

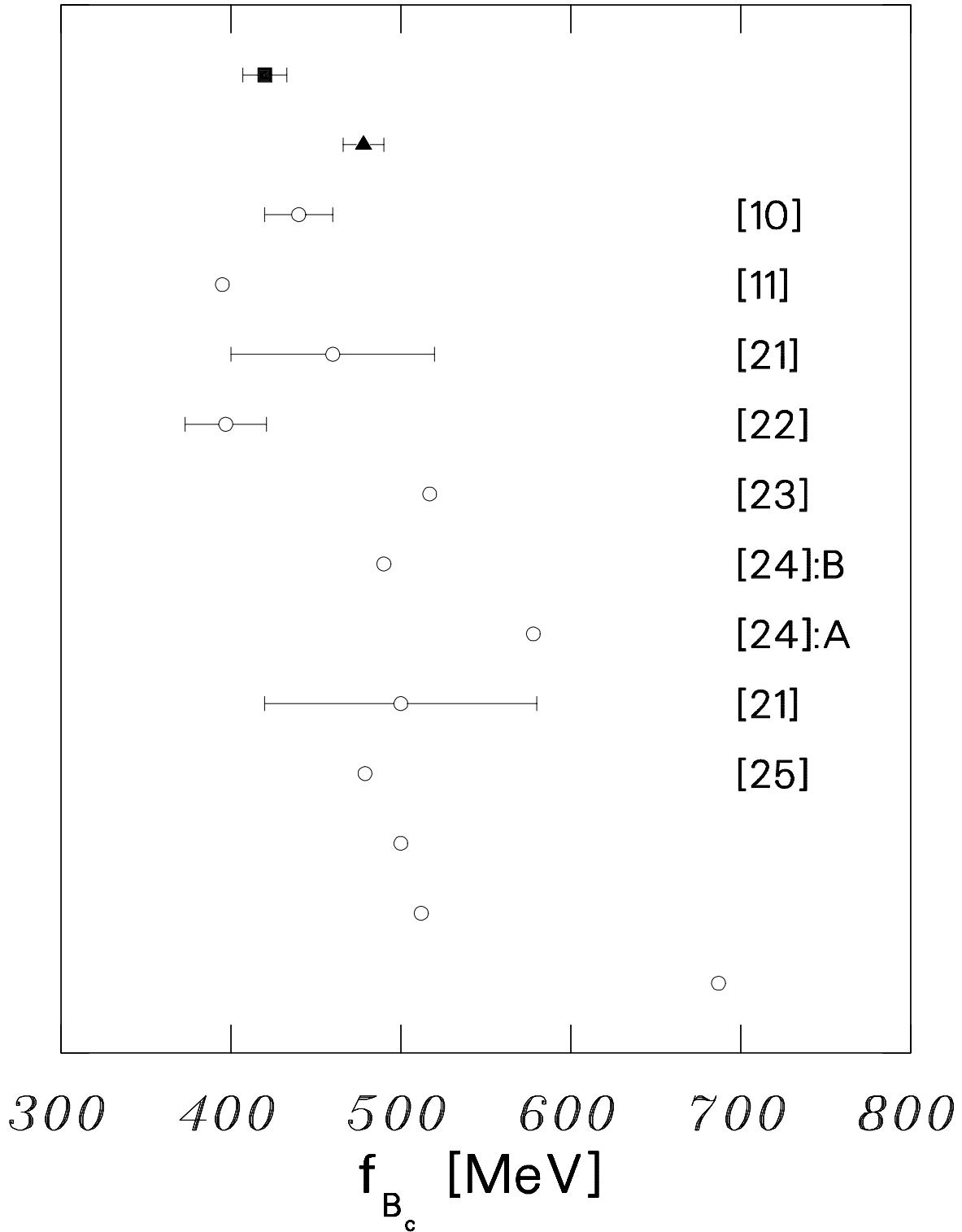


FIG. 5. A comparison with previous work. The filled square is this work: $\mathcal{O}(1, v^2)$; filled triangle is this work: $\mathcal{O}(1)$; and the open circles are other models labeled by their respective reference.

TABLES

TABLE I. Comparison of perturbative (one loop) and nonperturbative Landau links using the boosted definition of the coupling [see Eq. (10)]. Recall $u_0 = 1 - \alpha u_0^{(2)}$.

β	$u_0 = \left\langle \frac{1}{3} \text{ReTr} U_\mu \right\rangle$	$\alpha = 10/(4\pi\beta u_0^4)$	$u_0^{(2)}$	
			nonpert	pert
7.2	.805	.2632	.7409	.7503
7.3	.817	.2447	.7480	.7503
7.4	.8286	.2281	.7513	.7503

TABLE II. One-loop perturbative lattice NRQCD matching factors of quarkonia. Z_{match} is defined in and above Eq. (28). The results of the middle column are to be multiplied by $4/[3(2\pi)^4]$. The statistical error estimate from VEGAS is less than one percent.

ma[n]	$\delta\bar{V}_{lat} + \delta Z_{lat}^Q$	Z_{match}
1.4[3]	-43.9335	0.9141
1.5[3]	-42.3631	0.9037
1.6[3]	-45.3303	0.9049
2.1[2]	-49.3386	0.9274
2.2[2]	-49.8716	0.9235
2.3[2]	-50.3880	0.9192
2.8[2]	-52.8248	0.9359
2.9[2]	-53.2263	0.9323
3.0[2]	-53.7950	0.9288
3.5[2]	-57.0103	0.9462
3.6[2]	-57.5486	0.9437
3.7[2]	-58.3099	0.9416
4.2[2]	-61.5731	0.9574
4.3[2]	-62.3861	0.9564
4.4[2]	-63.3444	0.9558

TABLE III. One-loop perturbative lattice NRQCD matching factors of the B_c . Z_{match} is defined in and above Eq. (28). The results of the middle column are to be multiplied by $4/[3(2\pi)^4]$. The statistical error estimate from VEGAS is less than one percent.

$m_c a[n], m_b a[n]$	$\delta\bar{V}_{lat} + \delta Z_{lat}^c/2 + \delta Z_{lat}^b/2$	Z_{match}
1.4[3], 3.8[2]	-47.5372	1.0048
1.5[3], 4.4[2]	-47.2181	1.0096
1.6[3], 5.0[2]	-49.3620	1.0213

TABLE IV. M_{pert} versus M_{kin} for runs tuned to 6.35 GeV for the spin averaged B_c . The statistical error estimate of M_{pert} from VEGAS is less than one percent.

β	a(fm)	$m_c a[n], m_b a[n]$	$M_{\text{kin}} a$	$M_{\text{pert}} a$		$M_{\text{kin}}(\text{GeV})$
				w/o tad imp	w tad imp	
7.2	.204(1)	1.6[3], 5.0[2]	6.60(21)	6.91	6.92	6.37(21)
7.3	.185(2)	1.5[3], 4.4[2]	5.94(16)	6.15	6.28	6.32(18)
7.4	.163(3)	1.4[3], 3.8[2]	5.26(18)	5.42	5.67	6.37(24)

TABLE V. M_{pert} versus M_{kin} for runs nearest the charm and bottom regions respectively. The statistical error estimate of M_{pert} from VEGAS is less than one percent.

β	a(fm)	ma[n]	$M_{\text{kin}} a$	$M_{\text{pert}} a$		$M_{\text{kin}}(\text{GeV})$
				w/o tad imp	w tad imp	
7.2	.240(3)	1.6[3]	3.37(6)	3.17	3.89	2.77(6)
7.3	.205(3)	1.5[3]	3.20(5)	2.96	3.69	3.08(6)
7.4	.178(3)	1.4[3]	3.00(6)	2.80	3.55	3.32(9)
7.2	.198(2)	4.4[2]	9.07(21)	9.27	8.78	9.05(23)
7.3	.174(3)	4.3[2]	8.74(20)	9.06	8.63	9.91(28)
7.4	.151(2)	3.5[2]	7.05(20)	7.35	7.19	9.20(29)

TABLE VI. Vector decay constants of quarkonia (after including perturbative matching).

β	ma[n], $M_{\text{kin}} a$	a(fm)	f_V (MeV)	
			w/o v^2 rel cor	w v^2 rel cor
7.4	1.4[3], 3.00(6)	.178(3)	411(8)	364(9)
7.3	1.5[3], 3.20(5)	.205(3)	396(7)	352(8)
7.2	1.6[3], 3.37(6)	.240(3)	375(6)	335(8)
7.4	2.1[2], 4.33(10)	.164(2)	492(8)	464(10)
7.3	2.2[2], 4.50(7)	.188(2)	474(6)	446(8)
7.2	2.3[2], 4.69(8)	.220(2)	440(6)	415(8)
7.4	2.8[2], 5.66(15)	.156(2)	561(10)	541(12)
7.3	2.9[2], 5.84(11)	.179(2)	533(8)	515(10)
7.2	3.0[2], 6.06(13)	.208(5)	495(13)	477(14)
7.4	3.5[2], 7.05(20)	.151(2)	619(12)	605(14)
7.3	3.6[2], 7.26(15)	.174(2)	581(9)	567(11)
7.2	3.7[2], 7.52(17)	.201(2)	538(8)	524(10)
7.4	4.2[2], 8.51(29)	.149(2)	662(14)	651(15)
7.3	4.3[2], 8.74(20)	.174(3)	608(12)	597(13)
7.2	4.4[2], 9.07(21)	.198(2)	567(9)	557(11)

TABLE VII. B_c decay constants (after including perturbative matching).

β	a(fm)	f_{B_c} (MeV)	
		w/o v^2 rel cor	w v^2 rel cor
7.2	.204(1)	462(8)	407(11)
7.3	.185(2)	463(8)	406(10)
7.4	.163(3)	478(12)	420(13)